RATCHET CURRENT LANDSCAPE AT QUANTUM RESONANCE

A Thesis Presented to the Department of Theoretical and Applied Physics,

African University of Science and Technology, Abuja.

In partial fulfilment of the requirements for the award of

MASTER OF THEORETICAL AND APPLIED PHYSICS

By

KABIR SALIHU SURAJ

Supervised by

PD Dr. KENFACK ANATOLE

African University of Science and Technology

www.aust.edu.ng

P.M.B 681, Garki, Abuja F.C.T

Nigeria.

December, 2020.

RATCHET CURRENT LANDSCAPE AT QUANTUM RESONANCE

By

KABIR SALIHU SURAJ

A THESIS APPROVED BY THE DEPARTMENT OF THEORETICAL AND APPLIED PHYSICS

RECOMMENDED:

.....

Supervisor: PD Dr. Kenfack Anatole

.....

Head, Department of Theoretical Physics

APPROVED:

.....

Chief Academic Officer (Prof. C. E. Chidume)

.....

Date

DEDICATION

This thesis is dedicated to my beloved parents, Prof. Suraj Salihu and Assoc Prof. Rabi'atu Musa.

I pray that God Almighty be compassionate to both of them.

ACKNOWLEDGEMENT

My first gratitude goes to the Almighty God. Without His guidance, protection and wisdom I would not have been even close to where I am today.

This thesis is immensely indebted to the support and encouragement of many people: My thesis supervisor, PD Dr. Kenfack Anatole, who has been a constant source of inspiration, ideas and advice, and has always been incredibly generous with his time. Thank you very much Sir, for nurturing, mentoring and supporting me throughout my studies in AUST.

My sincere gratitude goes to Dr. Collins Akosa, Prof. Liverpool, Dr. Nelson Dzade, Dr. Theo Popov, Prof. Makinde and all my lecturers for their unceasing help and tutorship during my studies. Special thanks to Assoc. Prof. Idris Dauda for his unrelenting fatherly support.

Countless gratitude to my colleagues Ms. Jesutofunmi Fajemisin, Mr. Bonaventure Andrew, Mr. Gyang Chung, Mr. Denis Kiplangat for their collaboration, sharing of ideas and friendship.

A special thanks to my Thesis defense Committee and to Prof. / Dr. ... for raptly going through this thesis.

I would like to send my gratitude to the entire Staff and Management of AUST for their kindness and hospitality during my stay in AUST.

Finally, my wholehearted thanks go to my family: My mum, Salihu, Usman, Zainab, Sadiq, Muhammad, Hafsat and to Khadija Imam for the endless support and encouragement they all provide to me. I love you all.

DECLARATION

I, Kabir Salihu Suraj, declare that this work belongs to me. Every information I have derived from other sources, I have indicated in this thesis.

ABSTRACT

The ratchet effect is the rectified motion of atoms using an unbiased driving force. By ‘’unbiased’’ we mean to say that the time-average is equal to zero. This can be accomplished experimentally using cold atoms in a driven optical lattice.

This thesis describes the relationship between the Ratchet Current and other important parameters such as the kicking Potential P and effective Planck’s constant $\tilde{\hbar}$.

The thesis aims at investigating how resonances can be resolved in $\tilde{\hbar}$ and P spaces. The behavior of the number of current peaks as the kicking potential P increases was also investigated.

At the end, the thesis also explored how a tunable potential phase leads to current spikes as the Potential strength is amplified.

TABLE OF CONTENTS

LIST OF FIGURES

LIST OF TABLES

CHAPTER 1

GENERAL INTRODUCTION

The contents of this thesis fall within the general area of atomic and molecular optics. This is a very promising area of research for numerous Physicists. In this thesis, we concentrate on Ratchet Effect and its Applications.

THE RATCHET EFFECT

The ratchet effect is the production of directed motion out of unbiased fluctuations in periodic systems with broken symmetries. To elaborate on how this may be successfully achieved, we would begin by introducing The Feynman-Smoluchowski ratchet which is a classical thought experiment that demonstrates the idea behind the ratchet effect.

THE FEYNMAN-SMOLUCHOWSKI RATCHET

The Feynman-Smoluchowski ratchet is a device which was first considered by Smoluchowski in 1912 [1], and then made popular in 1964 by Feynman [2].

In that thought experiment, it was considered whether a ratchet and pawl could be used to convert the Brownian motion of particles to directed motion.

As we can see in figure 1, particles undergoing random motion turn a paddle wheel which is connected by an axle to a ratchet and pawl mechanism that constraints the system to rotate only in one direction.

Even though the Brownian motion of the particles averages to zero. This set-up seems (at first glance) that the random motion of the particles will cause the ratchet to eventually rotate in a specific direction [3].

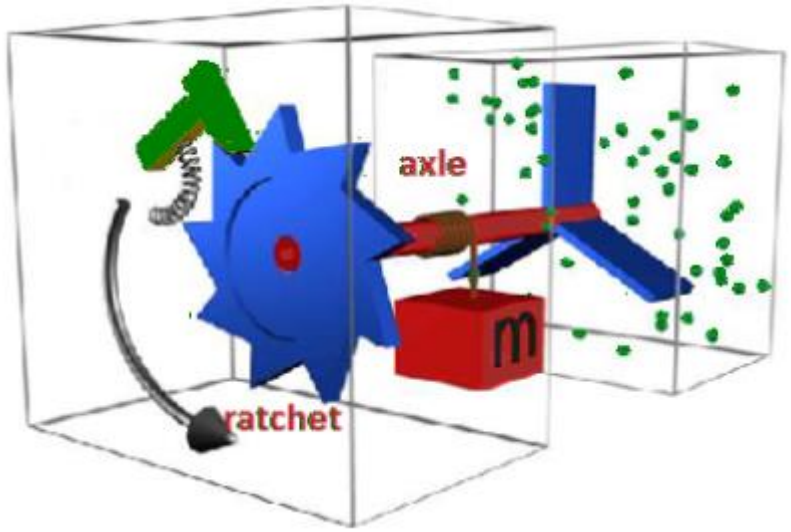

Figure 1: The Feynman-Smoluchowski ratchet.

The particles apply a torque on the paddle wheel and this rotates the ratchet. A mass m is attached to the axle so achieve work.

So this device seems to produce directed motion (rotation of ratchet) out of unbiased fluctuations (Brownian motion of particles). The problem, however, is that if such a device were to function, then it could be used to do useful work (for example lifting the mass m attached to the axle), and this would constitute a heat-engine at thermal equilibrium breaking the second law of thermodynamics. Feynman resolved this apparent dilemma by realizing that if the ratchet-pawl mechanism is sensitive enough to be affected by the Brownian motion of atoms, then the ratchet itself will also undergo Brownian motion. This means that even though the mechanism (the ratchet) is likely to rotate in one direction, it also has a tendency of rotating in the opposite direction because of its own Brownian fluctuations. Therefore, in thermal equilibrium the net motion remains zero and there would be no net work done so that second law of thermodynamics is obeyed [3].

To really understand how it works, it is pertinent to discuss the necessary conditions for ratchet effect to be achieved.

NECESSARY CONDITIONS FOR THE RATCHET EFFECT

The ratchet effect must satisfy two necessary conditions.

1. The system must be out of equilibrium.
2. There must be a broken symmetry in the system in order for there to be directed motion.

In the case of the Feynman-Smoluchowski ratchet this second requirement is fulfilled by the asymmetric teeth of the ratchet which ensures rotation is in one direction only

SOME SYSTEMS INVOLVING THE RATCHET EFFECT

Since the ratchet effect is common to systems that are out of equilibrium and have a broken symmetry, it can be found in a wide variety of systems, stretching from biological systems, physical systems, quantum systems and even financial systems. In what will follow, we will briefly identify some of these systems

MERCURY DROPS.

A force-free motion was experimentally achieved in a macroscopic system of mercury drop inside a capillary of asymmetric roughness. The system was subjected to an oscillatory electro capillary force of zero average value. The mercury drop is subjected to a potential whose shape gives the capillary roughness.

In some certain ranges of frequencies and intensities of the applied external force, the motion of the mercury drop is rectified. On time scales that are much larger than the period of the applied force, this motion is uniform. The average velocity of the drop is a function of the frequency and intensity of the external field. At a certain given frequency, there is an optimal value of the applied external force for which the average velocity is maximized [4]

PARTICLE PUMP.

In this scheme, the intrinsic sensitivity of the motion to the system parameters is used to provide the required ratchet motion.

The ratchet motion is sensitive to the diffusion constant which depends highly on the particle properties. Therefore, different particles can be manipulated in different ways. Under certain circumstances different particles can be made to move in opposite directions, providing separation mechanisms.

A quantum pumping mechanism which produces dc current in response to a cyclic deformation of the confining potential in an open quantum dot is reported in [5].

The voltage produced at zero current bias is sinusoidal in the phase difference between the two ac voltages. This deforms the potential and shows random fluctuations in amplitude and direction with small changes in external parameters such as magnetic field. There is a linear relationship between the amplitude of the pumping response and the frequency of this deformation.

Dependencies of pumping on the strength of the deformations, temperature, and breaking of time-reversal symmetry were also investigated.

BIOLOGICAL MOLECULAR MOTORS

The ratchet transport of biological molecular motors is responsible for muscle contraction in many living organisms. The protein motors are driven by chemical combustion and they undergo directed motion along an asymmetric landscape in a highly damped environment in the absence of any net force [3].

NANOWIRES

A conductivity study of Polypyrrole nanowires was performed [6]**.** The Nanowires have been prepared by a modest method that produces a varying doping concentration along the length of the wires. This variation gives rise to a ratchet effect which hinders the symmetry of the hopping

process of charges and hence the value of measured resistance of these nanowires becomes sensitive to the direction of current flow.

The asymmetry in resistance increases as the diameter of the nanowire decreases while it increases with increasing temperature.

This observation could be explained with the assumption that the spatial extension of the localized state involved in the hopping process is reduced as the doping concentration is reduced along the length of the nanowires.

The temperature dependence of the static dielectric constant $\epsilon \propto T^{-\delta}$ gave a value of δ as 1.4 instead of 1. This is probably due to dipole rotation being impeded in nanowires. This would also explain the observed reduction of ratchet effect with lowering temperature.

GRAPHENE

Impurities introduced by ad atoms give rise to the asymmetric potential. When driven by an electric field, a ratchet-like motion of the electrons occurs producing a measurable current [3].

Graphene possesses an intrinsic symmetry. When driven by a periodic electric field, no directed electric current should flow (since symmetry is not broken). However, if the graphene loses spatial symmetry due to its substrate or ad atoms, an electronic ratchet motion can be achieved. An experimental realization of such an electronic ratchet in graphene layers was demonstrated, proving the underlying spatial asymmetry [7].

An in-plane magnetic field induces the orbital asymmetry of the Dirac fermions, while the periodic driving comes from terahertz radiation.

The resulting magnetic quantum ratchet rectifies the alternating power into a direct current thus extracting work from the electrons which are out of equilibrium and driven by unbiased periodic forces.

CHAPTER 2

THEORETICAL BACKGROUND

This chapter presents some theoretical background for the topics in this thesis. It describes the atomic structure, laser cooling and trapping of neutral atoms, which was developed 50 years ago. It then presents the optical lattice, forms of driving, symmetry analysis treatment of the ratchet effect, which proves to be a powerful tool for determining the expected form of ratchet current.it finally describes the dependence of transport on some important parameters.

COOLING AND TRAPPING OF ATOMS

Due to their single valence electron, alkali metals such as rubidium and cesium are favored in modern laser cooling experiments as study cases since this makes them Bohr-like atoms [**3**].

Laser cooling manipulates the hyperfine states of the valence electron which are labelled by the F quantum number. The energy splitting between different hyperfine states is typically of the order of several hundred MHz to GHz. The hyperfine splitting of the cesium ground-state is used as a primary frequency standard to define the second. It has a value of 9.2 billion Hz, which is an exact value in virtue of the definition of the second.

Laser cooling refers to the use of laser fields to reduce the velocity of atoms. If we relate

$$\frac{1}{2}\mathrm{mv}^2 = \frac{1}{2}\mathrm{k_B T}$$

Where the LHS represents the atoms' average kinetic energy and the RHS represents their thermodynamic energy, we immediately see that their velocity falls with temperature. In this way, we describe slow atoms as 'cold' atoms and the process of slowing the atoms as 'cooling'.

Although laser cooling and trapping used to be a study in its own right [8], it is now used in many modern atomic physics experiments as a method of obtaining a cloud of cold atoms, which are subsequently ubiquitous. Laser cooling has become specifically popular since 30 years ago when

it was demonstrated that it can be used to cool atoms down to quantum degeneracy [9], as is done with Bose-Einstein Condensates. When a cloud of atoms is cooled to quantum degeneracy, the atomic de-Broglie waves become coherent and the entire cloud can be formally described by a single wave function, with the coherence length of this wave function extended over the entire ensemble. In some experiments this macroscopic coherence of the atomic cloud wave function is exploited to make quantum sensors such as gravimeters and gravity gradiometers [10]

BOSE-EINSTEIN CONDENSATE IN A RATCHET

A BEC is a phase transition that is obtained when atoms are slowed-down cooled to a state of quantum degeneracy. The atomic ensemble then starts to behave like a single coherent matter-wave. Since it has reached quantum degeneracy, a BEC in a ratchet would give rise to a quantum ratchet. This makes it a very intriguing subject on account of the peculiar features of a quantum ratchet, such as quantum resonances and a dependence on the initial driving phases [11, 12, 13]. One other feature of quantum ratchets that makes them very interesting is the existence of another transport mechanism for atoms in the lattice. This transport mechanism is ‘’quantum tunneling’’ which occurs between lattice sites.

BECs have a striking resemblance with solid-state physics and therefore can provide a test-bed for solid-state phenomena as.

One exciting similarity between BECs and Solid-state physics is the presence of vortices which occur in a BEC, which resemble the vortices occurring in a type-II superconductor associated to magnetic flux quanta. These vortices can be created in a BEC by rotating it. Once the rotation stops, the vortices remain in the BEC as a result of the superfluid state of the atoms [14].

Although the heart of a vortex represents an absence of the underlying fluid, the vortices display behaviors typically associated to particles, such as forming lattices with defects sometimes.[14] as well as nucleation of vortices [15]. The ratchet effect has already been observed with

superconducting vortices - or magnetic flux quanta - in solid-state systems [16.17], but seems challenging to observe for vortices embedded in a BEC. This is perhaps not surprising as it would be technically very difficult [3].

Observing the ratchet effect with the BEC and Examining the ratchet current of vortices in a BEC require distinct approach. For the ratchet effect with the BEC, the optical potential is been rocked, and then the BEC undergoes ratchet transport. This is rather confusing though, because strong perturbing rocking forces and near resonant fields are able to excite the BEC cloud and this will tamper with the quantum degeneracy. We resolve this problem by using a far-detuned optical lattice to provide a conservative potential; for an Rb BEC operating at 780 nm, a 1064 nm Nd-YAG laser is used. The above effect is however, distinct from a vortex ratchet. For a vortex ratchet, its potential landscape is the matter field that it sits in. So the rocking force should perhaps be supplied by the BEC itself acting on the vortices, and not by the optical potential acting on the BEC. In this way, it may be the internal vibrational state of the BEC that provides the rocking force to produce vortex ratchet transport. This internal rocking could perhaps be induced by displacing the BEC from the center of a harmonic trap, or even possibly may come about as a by-product of a ratchet driven BEC [3].

OPTICAL LATTICES

Optical lattices are formed when overlapping coherent laser beams interfere creating a spatially periodic polarization pattern.

In this arrangement, the light field produces a perfectly ordered array of nodes and anti-nodes which correspond to high and low intensity regions of the light field.

Optical lattices are typically classified depending on their type of detuning (far or near).

Far-detuned optical lattices provide a conservative (no dissipation) potential to trap atoms. Near-detuned lattices also trap atoms as well as providing a dissipative cooling mechanism – called Sisyphus cooling – that can cool atoms below the Doppler limit.

The difference between the two regimes arises as a result of the repressed scattering rate as the detuning is increased, since the scattering rate Γ^0 scales as the inverse square of the detuning

$$\Delta: \Gamma^0 \propto {}^{1}/_{\Delta^2}$$

LATTICE GEOMETRY

The lattice geometry is determined by two vital factors:

1. The orientation of the laser beams with respect to each other
2. The relative phases of the laser beams.

The period of the lattice is equal to half the wavelength of the lattice light, which is usually around a fraction of a micron. Therefore, a lattice formed from a beam with a width of several millimeters can have tens of thousands of lattice sites.

ONE DIMENSIONAL LATTICE

In general n + 1 beams are needed to form an n-dimensional lattice. A one dimensional lattice can be formed by counter-propagating beams with linear polarizations. To avoid any drift of the lattice due to drifting relative phases, the beams have to be phase-coherent. When the beams are coherent and their polarizations and have the same orientation, there is interference between the beams and a standing wave is formed with nodes and anti-nodes corresponding to constructive and destructive interference of the electric field. This forms a one-dimensional optical lattice.

TWO-DIMENSIONAL LATTICE

A two-dimensional lattice can be formed by overlaying two one dimensional lattices at transverse directions to each other. This would require four laser beams but instead we use just three laser beams orientated such that they lie in the same plane and mutually subtend an angle of 120° angle between them forming a hexagonal lattice.

In fact, using three beams instead of four is somewhat a necessity since the topography of an n-dimensional lattice is insensitive to phase-drifts only if it is formed from n+1 laser beams [18].

THE FORCE IN A LATTICE

The force experienced by the atoms in an optical lattice is produced by the potential gradient of the laser potential, corresponding to the light shift. This dipole potential gradient means that atoms are generally localized around lattice site minima, where the force reduces to zero. The Brownian motion random walk of an atom in a lattice corresponds to the atom scattering photons and moving stochastically across lattice sites.

The benefit of optical lattices is that they are perfectly defect-free as they are formed by light interference. Also they are highly tunable such that the lattice geometry can be changed drastically and in-situ. These two features are not true of solid-state lattices, and so optical lattices make an excellent candidate as a test-bed for concepts in solid-state physics.

SYMMETRY ANALYSIS

Let us consider a particle of mass m experiencing a spatially-dependent potential $U_0(x)$, subject to friction with coefficient γ, under the influence of a time dependent driving force $f(t)$, and subject to noise $\in(t)$. The equation of motion for this particle is given by the following Langevin equation:

$$m\ddot{x}=-\gamma\dot{x}-U_0(x)+f(t)+\in(t)$$

We can be rewrite this in terms of the momentum p as

$$\dot{P}=-\gamma\frac{P}{m}-U_0(x)+f(t)+\in(t)$$

The dot and prime denote differentiation with respect to time and space respectively.

In the case of cold atoms in an optical potential,

- The $\dot{P}$ term corresponds to the inertia;
- The $-U_0(x)$ term describes the dipole force due to the optical lattice potential;
- The $-\gamma\frac{P}{m}$ term corresponds to the optical damping due to Sisyphus cooling;
- The $f(t)$ term corresponds to the time-dependent driving force, implemented by modulating the lattice frequency;
- The noise term $\in(t)$ is the Brownian motion expressing the random walk of the atoms due to light scattering.

The purpose of this symmetry analysis is to find those symmetries of the equations of motion that forbid directed transport. By this knowledge of the conditions where transport is forbidden, we can move to regimes where these symmetries are broken so that transport is permitted.

In order to determine the symmetries of the system that forbid directed transport we consider transformations that reverse the particle's momentum such that

$$P\rightarrow -P$$

The reason we do this is because if the system (the Langevin equation) is invariant under such a transformation it means that

$$P=-P$$

And therefore

$$P\equiv 0$$

The momentum is zero and so directed transport is forbidden.

If the Langevin equation is invariant under such a transformation we say that the system is symmetric under that transformation. There are in fact two transformations that invert the momentum

$$P \to -P$$

Considering that the momentum is defined as

$$P = m\frac{dx}{dt}$$

Then the two transformations are

$$T_1: \qquad dx \to -dx \qquad dt \to dt$$

$$T_2: \qquad dx \to dx \qquad dt \to -dt$$

By integrating, we obtain:

$$T_1: \qquad x \to -x + x_0 \qquad t \to t + \tau$$

$$T_2: \qquad x \to x + \mu \qquad t \to -t + t_0$$

We will now apply these transformations to the Langevin equation in order to determine the regimes for which transport is forbidden.

In the following symmetry analysis we drop the noise term ξ from the Langevin equation since it is a symmetric Gaussian noise and so should not contribute to the long-time macroscopic drift velocity.

THE T_1 TRANSFORMATION AND "SHIFT-SYMMETRY"

Applying the $\mathbf{T_1}$ transformation

$$T_1: \qquad P \to -P \qquad x \to -x + x_0 \qquad t \to t + \tau$$

to the Langevin equation

$$\dot{P}=-\gamma\frac{P}{m}-U_0(x)+f(t)$$

It becomes

$$-\dot{P}=-\gamma\frac{-P}{m}+U_0(-x+x_0)+f(t+\tau)$$

Which implies that

$$\dot{P}=-\gamma\frac{P}{m}-U_0(-x+x_0)-f(t+\tau)$$

Using the fact that the optical potential is spatially symmetric

$$U_0(-x+x_0)=U_0(x)$$

a condition on the driving is obtained:

$$f(t+\tau)=-f(t)$$

Applying the transformation twice gives

$$f(t+2\tau)=f((t+\tau)+\tau)=-f(t+\tau)=f(t)$$

From this fact that

$$f(t+2\tau)=f(t)$$

it is deduced that

$$\tau==\frac{T}{2}$$

Where T is the characteristic time-period of the driving.

So the condition for the system to be symmetric under the T_1 transformation is that the driving has the form

$$f\left(t+\frac{T}{2}\right)=-f(t)$$

When the driving has this property we say the driving possesses “shift symmetry”.

THE T_2 TRANSFORMATION AND “TIME-REVERSAL SYMMETRY”

Applying the T_2 transformation

$$T_2: \qquad P \to -P \qquad x \to x+\mu \qquad t \to -t+t_0$$

to the Langevin equation

$$\dot{P}=-\gamma\frac{P}{m}-U_0(x)+f(t)$$

It becomes

$$\dot{P}=-\gamma\frac{-P}{m}-U_0(x+\mu)+f(-t+t_0)$$

To simplify this consider first the conservative case of a Hamiltonian ratchet where the damping term is zero. The following condition on the driving is then obtained:

$$f(-t+t_0)=f(t)$$

For the system to be invariant under the T_2 transformation.

When the driving obeys the above condition we say it possesses “time-reversal symmetry”. When the driving possesses shift-symmetry or time-reversal symmetry then transport is forbidden.

We now consider specific forms of the driving, and the conditions for them to be shift-symmetric and time-reversal symmetric

FORMS OF THE DRIVING FORCE

SINGLE HARMONIC DRIVING

Consider a periodic drive consisting of a single harmonic force

$$f(t) = \cos(\omega t + \varphi)$$

The driving is shift-symmetric

$$f\left(t + \frac{T}{2}\right) = -f(t)$$

for all φ because

$$\cos\left(\omega\left(t + \frac{T}{2}\right) + \varphi\right) = \cos(\omega t + \varphi + \pi) = -\cos(\omega t + \varphi)$$

Therefore transport is forbidden for this form of driving for all values of phase φ.

The situation changes, however, when we add an additional harmonic to form the biharmonic drive.

BIHARMONIC DRIVING

Consider a general periodic driving force formed from the sum of two harmonics

$$f(t) = A[\cos(\omega_1 t) + \varepsilon\cos(\omega_2 t + \varphi)$$

The frequency ratio can be written as

$$\frac{\omega_2}{\omega_1} = \frac{p}{q}$$

Where p and q are two co-prime integers (they share no common factors).

Since, by definition,

$$\omega_1 = \frac{2\pi}{T_1} \qquad \text{and} \qquad \omega_2 = \frac{2\pi}{T_2}$$

Then we have

$$\frac{p}{q} = \frac{T_1}{T_2}$$

Which means

$$qT_1 = pT_2 = T$$

Where T is the characteristic time-period of the driving.

We now look for when the driving is shift-symmetric such that

$$f\left(t + \frac{T}{2}\right) = -f(t)$$

We have

$$f\left(t + \frac{T}{2}\right) = A\left[\cos\omega_1\left(t + \frac{T}{2}\right) + \cos\omega_2\left(t + \frac{T}{2} + \varphi\right)\right]$$

$$= A\left[\cos\left(\omega_1 t + q\omega_1\frac{T_1}{2}\right) + \cos\left(\omega_2 t + p\omega_2\frac{T_2}{2} + \varphi\right)\right]$$

$$= A[\cos(\omega_1 t + q\pi) + \cos(\omega_2 t + p\pi + \varphi)]$$

It can be seen that if p and q are both odd, then

$$f\left(t + \frac{T}{2}\right) = -f(t)$$

And the driving is shift-symmetric. So no transport can occur if p and q are both odd. Since we know that p and q aren't both even, as they were defined as co-prime integers, we can deduce that p and q must have opposite parity in order for the shift-symmetry to be broken.

Let us now consider when the driving is time-reversal symmetric such that

$$f(-t + \tau) = f(t + \tau)$$

for some time τ , which is exactly equivalent to

$$f(-t + \tau) - f(t + \tau) = 0$$

$$f(-t+\tau) = A[\cos(-\omega_1 t + \omega_1 \tau) + \epsilon\cos(-\omega_2 t + \omega_2 \tau + \varphi)]$$

$$= A[\cos(\omega_1 t - \omega_1 \tau) + \epsilon\cos(\omega_2 t - \omega_2 \tau - \varphi)]$$

and

$$f(t+\tau) = A[\cos(\omega_1 t + \omega_1 \tau) + \epsilon\cos(\omega_2 t + \omega_2 \tau + \varphi)]$$

Subtracting the two equations gives us terms like

$$\cos(\alpha - \beta) - \cos(\alpha + \beta)$$

for which we can substitute

$$2\sin\alpha\sin\beta$$

to get:

$$f(-t+\tau) - f(t+\tau) = 2A[\sin(\omega_1 t)\sin(\omega_1 \tau) + \epsilon\sin(\omega_2 t)\sin(\omega_2 \tau + \varphi)] = 0$$

Since the time-reversal symmetry must hold for all time t we have the conditions

$$\sin(\omega_1 \tau) = \sin(\omega_2 \tau + \varphi) = 0$$

Therefore

$$\omega_1 \tau = m\pi \qquad \text{and} \qquad \omega_2 \tau + \varphi = \overline{m}\pi$$

for integers m and $\overline{m}$

Substituting

$$\omega_2 = \frac{p}{q}\omega_1 \tau = \frac{p}{q} m\pi$$

into the second line and multiplying through by q gives the condition:

$$q\varphi = (q\overline{m} - pm)\pi$$

We let $(q\overline{m} - pm) = n$

where n is an integer

Then

$$q\varphi = n\pi$$

Therefore, the driving is time-reversal symmetric when $q\varphi = n\pi$ for n integer,

And we expect to see no transport at these values of φ. This suggests that a function describing the transport $v_c(\varphi)$ will have zeros at $q\varphi = n\pi$, which implies that the velocity measurements will have some periodic structure corresponding to the time-reversal symmetry breaking governed by φ. We note that if the first harmonic had a phase φ_1, then the conditions would become

$$\omega_1\tau + \varphi_1 = m\pi \qquad \text{and} \qquad \omega_2\tau + \omega_2 = \overline{m}\pi$$

Upon substituting

$$\omega_2\tau = \frac{p}{q}\omega_1\tau = \frac{p}{q}m\pi - \frac{p}{q}\varphi_1$$

We would get the condition:

$$q\left(\varphi_2 - \frac{p}{q}\varphi_1\right) = q\varphi_r = n\pi$$

Where we have defined the relative phase

$$\varphi_r = \varphi_2 - \frac{p}{q}\varphi_1$$

Therefore, we see that the time-reversal symmetry condition of

$$q\varphi = n\pi$$

Applies to the relative phase. Usually we take

$$\varphi_1 = 0$$

So that the relative phase is determined by $\varphi_2 = 0$

QUANTUM RESONANCE

This occurs when the flashing period coincides with the recoil frequency. It is related to the arithmetic nature of the effective Planck constant h of kicked systems. Resonances occur specifically if

$$\tilde{\hbar} = 4\pi\frac{\mathrm{r}}{\mathrm{s}}$$

Where r and s are mutually prime integers. Cases with small s are called low-order quantum resonance (LOQR) while those with large values of s can be called high-order quantum resonance (HOQR).

Low-order quantum resonances manifested by directed currents have been realized with cold atoms. It has also been shown that by increasing the strength of an experimentally achievable delta-kicking ratchet potential, quantum resonances of a very high order may naturally emerge and can induce larger ratchet currents than low-order resonances, with the underlying classical limit being fully chaotic.

THE SYSTEM

Here we consider in dimensionless units, the following Schrödinger equation [19]

$$\mathrm{i}\tilde{\hbar}\frac{\partial\psi}{\partial\mathrm{t}} = -\frac{\tilde{\hbar}^2}{2}\frac{\partial^2\psi}{\partial^2\mathrm{x}} + \mathrm{v}(\mathrm{x})\sum_{\mathrm{l}=0}^{\infty}\delta(\mathrm{t}-\mathrm{l})\,\psi$$

Where x is the position, and $\mathrm{v}(\mathrm{x})$ is the potential which is given by

$$\mathrm{v}(\mathrm{x}) = \mathrm{K}[\sin(\mathrm{x}) + \alpha\sin(2\mathrm{x})]$$

And is assumed to be periodically flashed off and on with delta kicks. Here t is the time variable and l an integer that counts the number of kicks.

Such a dissipation-less ratchet potential $v(x)$ has been successfully engineered by superimposing a conventional standing wave potential of λ/2 spatial periodicity with a fourth-order lattice potential of λ/4 periodicity, [20].

CHAPTER 3

METHODOLOGY AND COMPUTATIONAL DETAILS

SOLVING THE SYSTEM

THE FAST FOURIER TRANSFORM SPLIT OPERATOR METHOD

This method, which was developed by Feit and Fleck in the 1980's is a method of solving the time dependent Schrödinger equation [21]. It is a spectral method known as the Split Operator Method.

The time dependent Schrödinger equation (TDSE) is given by

$$i\hbar\frac{d\psi(x,t)}{dt} = -\frac{\hbar^2}{2m}\frac{d^2\psi(x,t)}{d^2x} + v(x)\psi(x,t)$$

The evolution of the wave function within an infinitesimal time interval Δt can be written as:

$$|\psi(t+\Delta t)\rangle = \hat{U}(t+\Delta t,t)|\psi(t)\rangle$$

Where

$$\hat{U}(t+\Delta t,t) = \exp\left(-\frac{i}{\hbar}\hat{H}\Delta t\right)$$

Is a unitary evolution operator containing the exponential of the Hamiltonian Operator.

$$\hat{H} = \hat{T} + \hat{V}$$

Which we can split into products of exponentials for a small but finite Δt:

$$\exp\left(-i\hbar\hat{H}\Delta t\right) = \exp\left(-i\hbar\,\hat{V}/_2\,\Delta t\right)\exp\left(-i\hbar\hat{T}\Delta t\right)\exp\left(-i\hbar\,\hat{V}/_2\,\Delta t\right) + O(\Delta t^3)$$

Or equivalently

$$\exp\left(-i\hbar\hat{H}\Delta t\right) = \exp\left(-i\hbar\,\hat{T}/_2\,\Delta t\right)\exp\left(-i\hbar\hat{V}\Delta t\right)\exp\left(-i\hbar\,\hat{T}/_2\,\Delta t\right) + O(\Delta t^3)$$

This replacement is not exact since $[\hat{T},\hat{V}] \neq 0$. The associated commutation error which is third order in Δt, $[O((\Delta t)^3)]$ can be made acceptably small if Δt is chosen to be sufficiently negligible.

The operator product on the right-hand side of the two equations above has the following advantages

(i) It is symmetric under time-reversal

(ii) it is unitary

(iii) It is easy to implement

It is thus easy to implement because of the following reason: The operator containing the potential is applied by simply multiplying in configuration space. In the same fashion, the operator containing the exponential of the kinetic energy is applied through multiplication in momentum space

The credit for the above expansion of the two equations goes to Baker, Campbell and Hausdorff for their formula for the exponential of an operator:

$$\exp\left(t(\hat{A}+\hat{B})\right) = \exp\left(t\hat{A}\right)\exp\left(t\hat{B}\right)\exp\left(-\frac{t^2}{2!}[\hat{A},\hat{B}]\right)\exp\left(-\frac{t^3}{3!}(2\left[\hat{B},\left[\hat{A},\hat{B}\right]\right]+\left[\hat{A},\left[\hat{A},\hat{B}\right]\right]\right)\ldots$$

To the third order with $t = 1$.

A Fourier transformation is used to move from the momentum-space representation of the wave function to the configuration space representation and vice versa. For example, in the case of a one-dimensional single particle function, we have

$$\psi\left(\hat{P}\right) = \int \psi(x)\exp\left(-\frac{i}{\hbar}px\right)dx$$

With this notation, the momentum-space wave function is normalized to 2π. We represent the wave function on a grid with a finite number of points. The efficient Fast Fourier Transformation

(FFT) algorithm is then applied. Employing the FFT, the computational time for one Fourier transform is proportional to $N \times \log N$, where N is the number of grid points. Using the conventional evaluation of the discrete Fourier transform, the computational effort scales with N^2 because for each of the N grid points in momentum space, a sum over N positions in coordinate space has to be calculated. The application of the operators $\exp\left(-\frac{i}{\hbar}\Delta t\hat{V}\right)$ and $\exp\left(-\frac{i}{\hbar}\Delta t\hat{T}\right)$ requires N multiplications, each. Thus, for large N, the FFT is the element that mainly determines the computational time.

One should note however, that the favorable FFT scaling applies only when the number of grid points is a product of small prime numbers; ideal is the case N^{2N} .

COMPUTING THE GROUND STATE

In practice, we usually start the computation with the ground state of the unperturbed system as our initial state. The most convenient way to obtain this ground state is the “relaxation method”:

We begin with an arbitrary wave function $\Psi(t = 0)$and propagate it using the scheme describe above but in imaginary time

$$t = i\tau$$

This is the so-called the imaginary time propagation.

In terms of the Eigen states $|n\rangle$ with energies E_n, the evolution over an interval $\Delta\tau$ is given by

$$\Psi(\tau + \Delta\tau) = \sum_k \langle n|\Psi(\tau)\rangle \exp(-E_n\Delta\tau)|n\rangle$$

In complete analogy to the propagation in real time we use the split-operator method as described above. It clearly turns out that the state with the lowest energy suffers less damping than the excited states. In practice, the wave function is renormalized in each time step so that after a

sufficient number of steps, the normalized ground-state wave function Ψ0 is obtained. The corresponding energy

$$E_0 = \lim_{\tau \to +\infty} -\frac{1}{2\Delta\tau} \ln \frac{\langle \Psi(\tau + \Delta\tau) | \Psi(\tau + \Delta\tau) \rangle}{\langle \Psi(\tau) | \Psi(\tau) \rangle}$$

Can be used as convergence criterion because it converges simultaneously with the wave function. The relaxation method may be employed to determine excited states as well. To achieve this, all Eigen states with lower energies have to be determined first. Then, these states must be projected out in each time step.

ABSORBING BOUNDARY CONDITIONS

Often, the numerical grid cannot be made large enough to contain the whole wave function. In particular, this is so when we deal with ionization in strong fields: Within a few optical cycles, the extension of the electronic wave function easily reaches several hundred atomic units. Numerically, wave packets reaching the grid boundary must be absorbed. Otherwise, a "ghost" wave packet reenters on the opposite side of the grid since the numerical Fourier transformation effectively imposes periodic boundary conditions. In propagation techniques other than the split-operator method, one usually has to specify the boundary conditions explicitly. In that case, the absence of an absorber typically leads to reflection. Adding an imaginary ("optical") potential to the external potential is a convenient way to achieve absorbing boundary conditions. For example, on a one-dimensional grid extending from $-x_0$ to x_0 , one can use an optical potential of the form

$$V_{opt(x)} = \begin{cases} i\lambda(x + x_1)^2 & \text{if } -x_0 \le x < -x_1 \\ 0 & \text{if } -x_1 \le x < x_1 \\ i\lambda(x - x_1)^2 & \text{if } x_1 \le x < x_0 \end{cases}$$

With the parameter λ describing the strength of absorption. Adding this optical potential to the potential $\hat{V}(x,t)$ is equivalent to effectively multiplying the wave function in the regions $[-x_0, -x_1]$ and $[x_1, x_0]$ by $\exp(-\lambda(x \pm x_1)^2)$ in each time step. Therefore, instead of employing an optical

potential, one can equivalently multiply in every time step with an absorbing mask function “by hand.” This is what one must do if a splitting technique is used where the outgoing wave packets are transferred to an outer grid and propagated further in time. The parameter λ has to be chosen with care: If λ is too small, the wave packets are not entirely absorbed before they run into the boundary. On the other hand, if λ is too large, a part of the wave function is reflected. This is similar to the behavior of a wave propagating along a rope with fixed ends.

CHOOSING THE GRID SPACING AND THE TIME STEP

The correct grid spacing, the grid size, and the size of the time step must be chosen for the numerical propagation. More accurate results are obtained with smaller steps and larger grids but this increases the computation time and use of memory.

Generally, all results are cross-checked to ensure that they remain stable whenever these parameters are upgraded.

In addition, hints for estimating the minimum requirements can be given based on the classical electronic motion described above.

1. With an electronic grid spacing Δx, the extension of the momentum-space grid is

$$[-p_{max}, -p_{max}] \qquad \text{with} \qquad p_{max} = {}^{\pi}/_{\Delta x}$$

Since the maximum momentum that an electron can receive classically is ${}^{2E_0}/_{\omega}$ In a strong laser, the extension of the momentum-space grid must be larger than ${}^{2E_0}/_{\omega}$

2. At least during the time between ionization and recollision, the size of the grid along the electronic coordinates must be large enough to encompass all oscillatory motions of the electrons in the laser field. Thus, the minimum range is −2α to 2α, where α is the classical oscillation amplitude.

3. Using a time step Δt, the maximum representable energy difference is

$$\Delta E = {}^{2\pi}/_{\Delta t}$$

This value has to be larger than the difference between the maximum energy E_{max} and the ground-state energy.

If we inserting the maximum drift velocity ${}^{E_0}/_{\omega}$ of an electron in a laser field into the kinetic energy expression, we obtain $E_{max} = 3U_p$ per each electron.

It is however important to note that the time step derived from this argument is in most cases much larger than the time step required for an accurate propagation with the split-operator method.

Typical parameters for the calculations in this thesis are:

- Grid size
  - – Electronic coordinates: 100 to 400 a.u.
  - – Nuclear separation: 10 to 80 a.u. ˆ
- Spatial step size
  - – Electronic coordinates: 0.2 to 0.4 a.u.
  - – Nuclear separation: 0.1 a.u. ˆ
- Temporal step size
  - – Time step: 0.05 a.u

ALPHA

The parameter α determines how the potential is skewed.

$$\alpha = \frac{V_2}{V_1} \text{ and } \qquad K = \frac{V_1}{2}$$

Where V_1 and V_2 denote the potential depths of the lattice harmonics λ/2 and λ/4, respectively.

With α ∈ (0, 0.5] the saw teeth of the potential lean left, stimulating the transport to the right for classical diffusive motion. While it leans to the right if α ∈ (0.5, 1], stimulating the transport to the left for classical diffusive motion. The familiar rotor potential can be recovered for α = 0.

For this temporally-symmetric system, the ratchet effect is only possible for broken spatial symmetry, i.e., for α not = 0. We use scaled units here with both the spatial L and the temporal T periods set to unity.

EFFECTIVE PLANCK CONSTANT

The quantum nature of the system is in the effective Planck constant

$$\widetilde{\hbar} = 8\omega_{\mathrm{R}}\mathrm{T}$$

Which varies as one alters the pulsating period T.

Here,

$\omega_{\mathrm{R}} = \frac{\widetilde{\hbar}\mathrm{K}_{\mathrm{L}}^{2}}{2\mathrm{m}}$ Is the recoil frequency of the applied laser field, with m the atom mass and K_{L} the photon wave number that makes up a lattice period of $(2\mathrm{K}_{\mathrm{L}})^{-1}$ for the optical potential.

THE QUANTUM MAP

The quantum map of the above delta-kicked ratchet model is given by

$$\widehat{\mathrm{U}} = \exp\left(-\mathrm{i}\widetilde{\hbar}\widehat{\mathrm{k}}^{2}/_{2}\right)\exp\left(-\mathrm{iPv}(\hat{\mathrm{x}})\right)$$

Where $\hat{\mathrm{x}}$ and $\widehat{\mathrm{k}} = -\mathrm{i}\frac{\partial}{\partial \mathrm{x}}$ represent the position and the wave number operators, respectively. Here we have also define $\mathrm{P} = \mathrm{K}/_{\widetilde{\hbar}}$ for later use. All computational examples presented below are for fixed skewness parameter α = 0.3

CHAPTER 4

RESULTS AND DISCUSSION

In this section I have reproduced the results obtained by Anatole Kenfack et al [22]. I proceeded to investigate how the Number of resonant peaks is affected by the kicking strength. I also explored the ratchet current landscape to recover more resonances. I finally probed the variation of current as a phase angle is tuned.

THE RATCHET CURRENT,

The ratchet current Denoted $\langle k \rangle$ is defined as the expectation value of the wave number operator $\hat{k}$. Its relationship with time is shown in Fig 2, for different values of the potential strength P and for specific values of the effective Planck's constant. One readily sees that there is no directed transport for all the values of the potential strength when

$\tilde{\hbar} = 1.001\pi$

By sharp contrast, the current acceleration may be strongly favored in the positive or negative direction as illustrated in Fig 3, 4, and 5, where

$\tilde{\hbar} = 0.7\pi$ for (r, s) = (7, 40),

$\tilde{\hbar} = 2.625\pi$ for (r, s) = (21, 32),

$\tilde{\hbar} = 1.5\pi$ for (r, s) = (3, 8), respectively

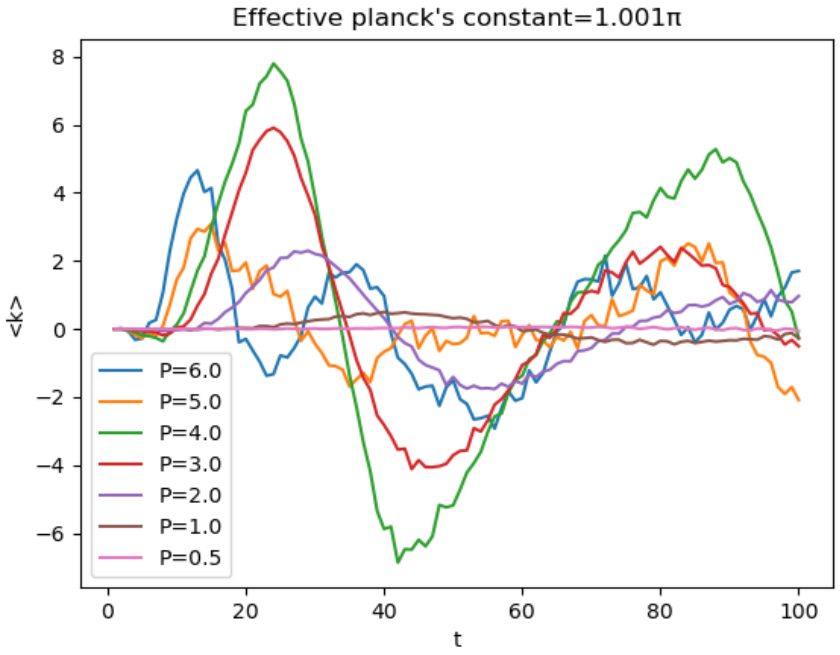

Figure 2: Time depence of current for $\tilde{\hbar} = 1.001\pi$

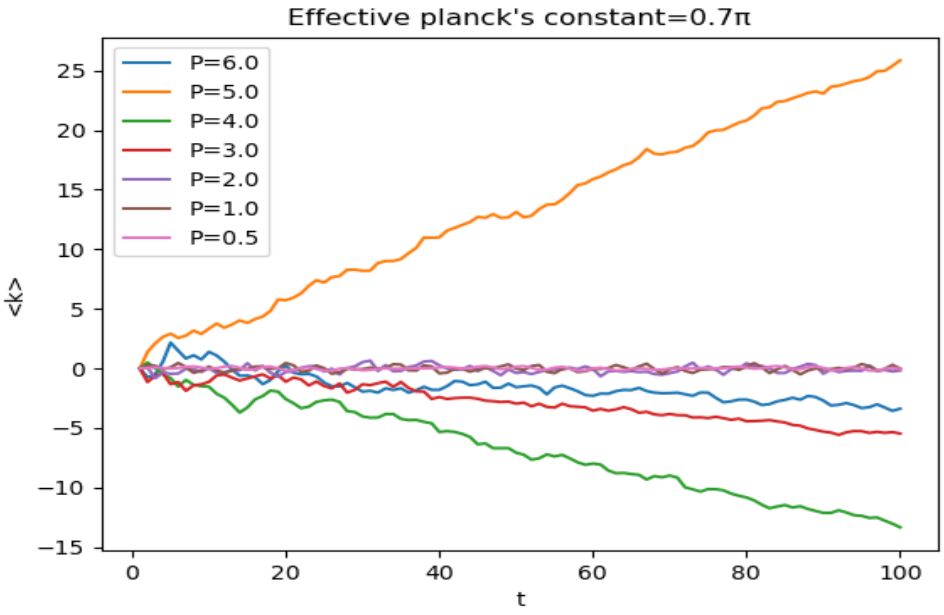

Figure 3 : Time depence of current for $\tilde{\hbar} = 0.7\pi$

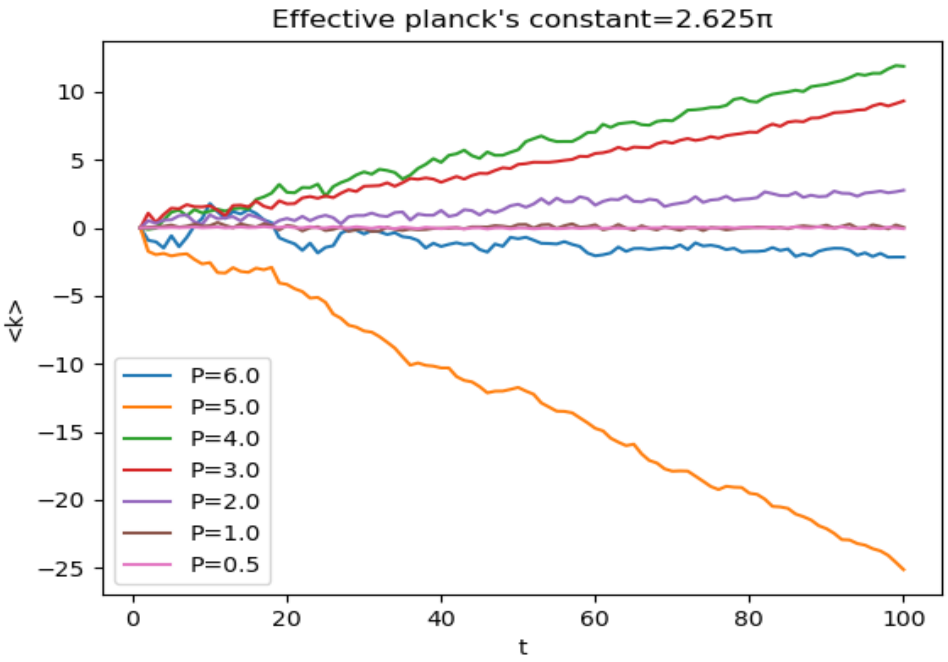

Figure 4: Time depence of current for $\tilde{\hbar} = 2.625\pi$

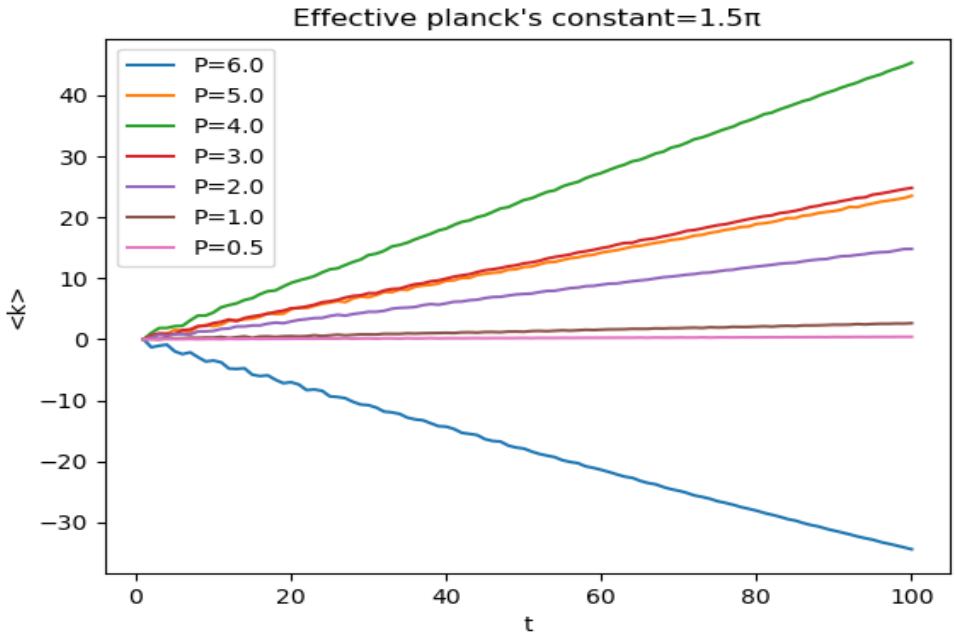

Figure 5 : Time depence of current for $\tilde{\hbar} = 1.5\pi$

TIME DEPENDENCE OF THE RATCHET CURRENT FOR DIFFERENT VALUES OF P AND $\tilde{\hbar}$

From graphs below we can see that

(a) At off-resonance $\tilde{\hbar} = 1.001\pi$, no directed transport occurs for any value of P.

(b) At resonance $\tilde{\hbar} = 0.7\pi$ with the tuple (r, s) = (7, 40); transport occur in either direction, at P-dependent acceleration rates.

(c) At resonance $\tilde{\hbar} = 2.625\pi$ (r, s) = (21, 32).

(d) At resonance $\tilde{\hbar} = 1.5\pi$; (r, s) = (3, 8).

We will now like to see how the current is affected by the effective Planck's constant. In figures 6,7,8,9, the ratchet current ⟨k⟩ as a function of $\frac{\tilde{\hbar}}{\pi}$ after 200 kicks, with the potential parameter α = 0.3 and different potential strengths is shown.

Figs 10 and 11 represent HOQRs.

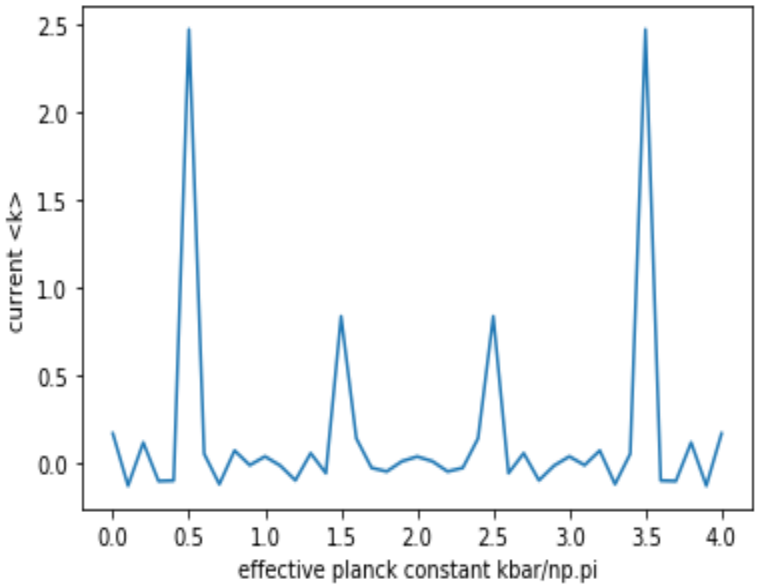

Figure 6 : Current against Effective Planck's constant for P=0.5

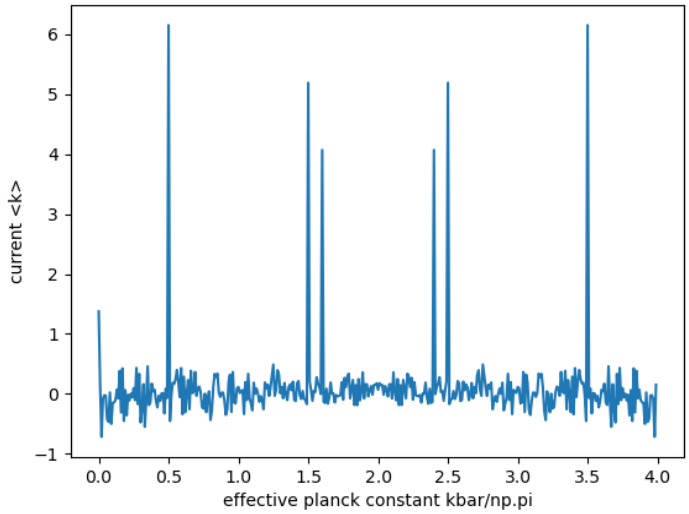

Figure 7: Current against Effective Planck's constant for P=1.0

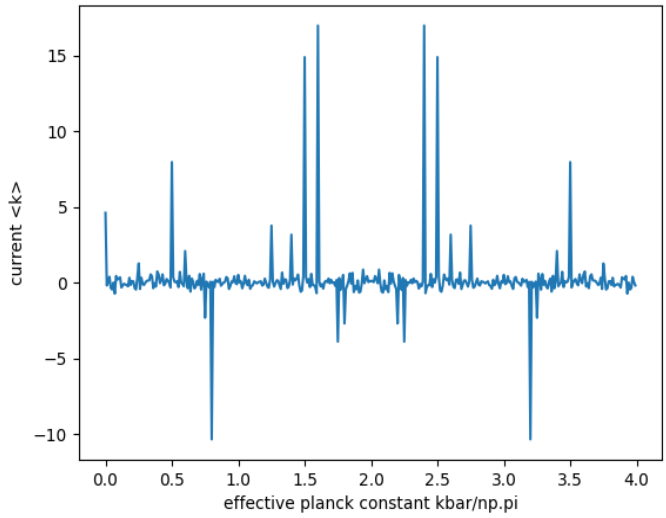

Figure 8 : Current against Effective Planck's constant for P=2.0

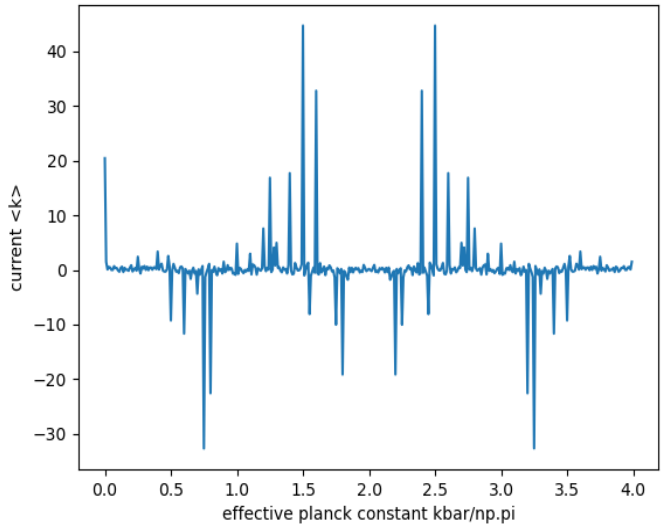

Figure 9: Current against Effective Planck's constant for P=2.5

In fig 6, main resonances appear with low P. As P increases in 7, 8, and 9, full chaos is being developed and significant ratchet currents due to higher-order quantum resonances emerge.

Figures 6,7,8,9 display the ratchet current as a function of the effective Planck's constant after 200 kicks or temporal periods.

In Fig 6, P = 0.5 and the results match the findings of [19], showing a net drift at those quantum resonances where the $\frac{\tilde{\hbar}}{\pi}$ has half integer values.

As the strength P is increased, the system exhibits dramatic changes. For example, when P = 1.0 in Fig 7, two twin peaks emerge.

One can also see as shown in Fig.8 and 9 that larger values of P lead to

1. Proliferation of peaks: the number and strength of resonant peaks rapidly increase as we increase the strength
2. Current reversals: there is directed transport in the opposite direction

As shown in Table I, many of these peaks are found to be associated with very high-order quantum resonances covering a wide range of r and s. Remarkably, these high-order resonances may yield larger ratchet current acceleration than the main resonances, and in either case the current direction depends on P.

It is very important to note however, that HOQRs do not always transport better than LOQR. Compare, for example, the HOQR at $\frac{\tilde{\hbar}}{\pi}$ = 0.6 to the LOQR at $\frac{\tilde{\hbar}}{\pi}$ = 0.5, 1.5, 3.5.

Figures 6,7,8,9 also show that relatively small changes in $\tilde{\hbar}$ can dramatically change the ratchet current, thus experimentally offering a means of isolating different HOQRs. This also suggests that particles with slightly different masses, hence slightly different $\tilde{\hbar}$ and different P due to an isotope effect, may display qualitatively different kinds of transport. Neglecting at the moment the non-ideal situation in experiments, note that the resonance peaks shown in the figures are better resolved with increasing kicks since the absolute amplitude of the current peaks is proportional to the number of kicks.

Table 1: Some high-order resonances in Fig.12

$\frac{\tilde{\hbar}}{\pi}$	0.6	0.7	0.75	1.125	1.55	3.3
(r, s)	(3,20)	(7,40)	(1,16)	(9,32)	(31,80)	(33,40)

POSSIBILITY OF EXPERIMENTALLY OBSERVING HOQR PEAKS.

Using constraints associated with state-of-the-art experiments A. Kenfack et al have carried out extensive computations verifying that the above observed HOQR ratchet current can be clearly observed in experiments, at least for time scales of 20 − 30 kicks. In particular, the ratchet currents are sufficiently stable when

(i) considerable dephasing is present

(ii) A finite pulse-width instead of delta-kicks is considered, and

(iii) A realistic quasi-momentum spread in the initial state is considered.

For example, for the case of $\tilde{\hbar}$ = 2.625π, P = 5.0 shown in Fig.4, we find that the HOQR ratchet current deviates considerably from the ideal case only after about 20 kicks, for a realistic quasi-momentum spread as estimated in [25]. It was also checked that if a superposition state of momentum is used as the initial state, then a HOQR ratchet current can be also effectively demonstrated without using a bichromatic optical lattice.

CLASSICAL DYNAMICS OF THE MODEL SYSTEM

We would now briefly describe the classical dynamics of the model system. With the classical stochasticity parameter or kick strength

$$K = \tilde{\hbar}P,$$

The associated classical map is given by

$$p_{l+1} = p_l - K[\cos(x_l) + 2\alpha\cos(2x_l)]$$

$$x_{l+1} = x_l + p_{l+1}$$

Where p_l is the momentum variable conjugated to the coordinate x_l . Figure 10 displays the classical phase space for α = 0.3 and for varying K. As K is increased, the islands which initially dominated the phase space become smaller and reduce in number as is clear in Fig. 10 (a), (b), (c)]. This trends until a threshold value K_{thr}, when essentially full chaos is reached In Fig.10(d) where

K = 0.8π > K_{thr},

K_{thr} ≈ 0.75π

The entire phase space is then seen to be fully chaotic.

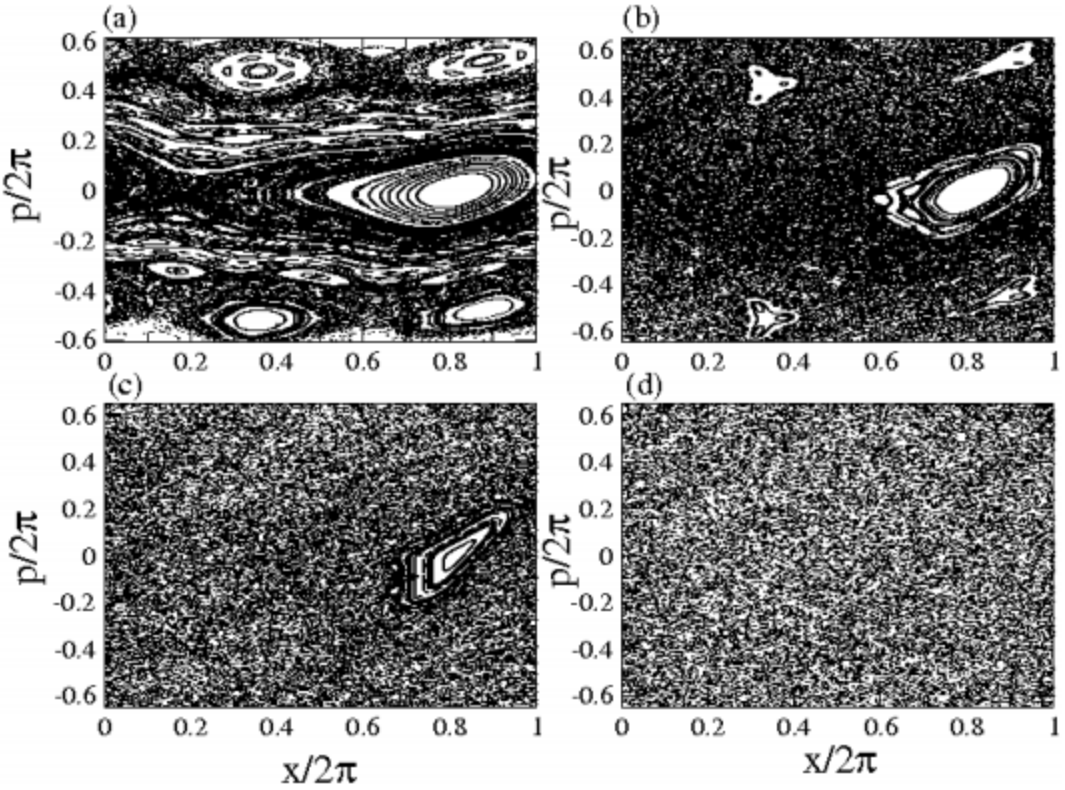

Figure 10: Classical phase space structures for the kicked ratchet map

Figure 10 shows the Classical phase space structures for the kicked ratchet map for α = 0.3 showing regular islands embedded in the chaotic sea for (a) K = 0.25π, (b) K = 0.55π and (c) K = 0.70π. In panel (d) K = 0.8π and full chaos is reached.

It is note-worthy that clear High Order Quantum Resonance peaks only emerge when the classical counterpart is fully chaotic. This observation has been verified by tuning the parameter α between 0 to 10, with different threshold value $\mathrm{K_{thr}}$.

A fascinating connection between a phenomenon that is purely quantum and another which is purely classical deserve of some annotations. In the time being though a profound explanation may not exist.

Continuous energy bands can result from Quantum resonances [26]. A potential of height P = K/$\tilde{\hbar}$ supports only a certain number of energy bands denoted n, that are below the potential barrier. As the well deepens, n increases with K, specifically as shown in Fig.11

$$n \propto \sqrt{K}$$

For a fixed $\tilde{\hbar}$ = K/P.

Larger values of K corresponds to more classical chaos, and leads to more bands that can contribute to transport, whence a HOQR is more likely to be detected.

Alternatively, as we increase K for fixed P, n increases, leading to more resonant values $\tilde{\hbar}$ being available.

Both ways, we see more peaks in the plot of the ratchet current against $\tilde{\hbar}$. As such, chaos and HOQRs, both requiring sufficiently large K, go hand-in-hand, an interesting result also noticed [27] using other signatures.

Since classical chaos arises through the growth of nonlinear resonances [28], its connection with HOQRs might exist at a deeper level.

Finally, note that for our Hamiltonian ratchet model, directed transport may occur for n < 2, albeit being weaker than in cases with larger n. This is in contrast to dissipative systems [29], where the ratchet effect exists only if there are at least two bands below the barrier.

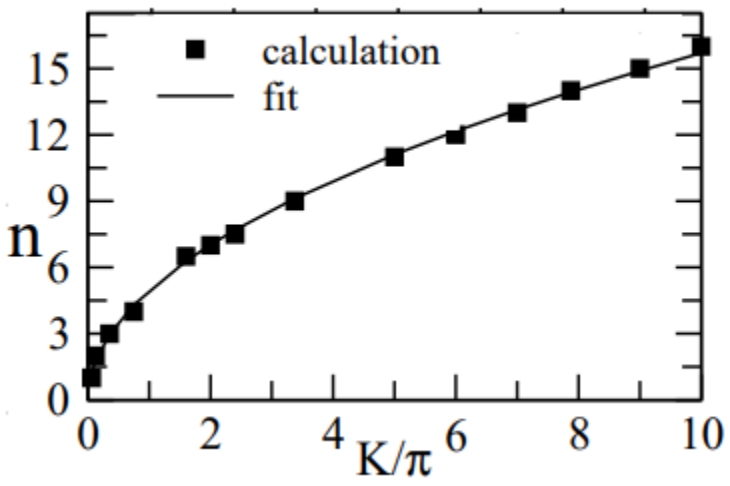

Figure 11 : The number of Floquet bands below the potential barrier as a function of K.

THE AVERAGE CURRENT ACCELERATION RATE

The average current acceleration rate is given by

$$\Gamma \equiv \frac{\langle k \rangle}{l}$$

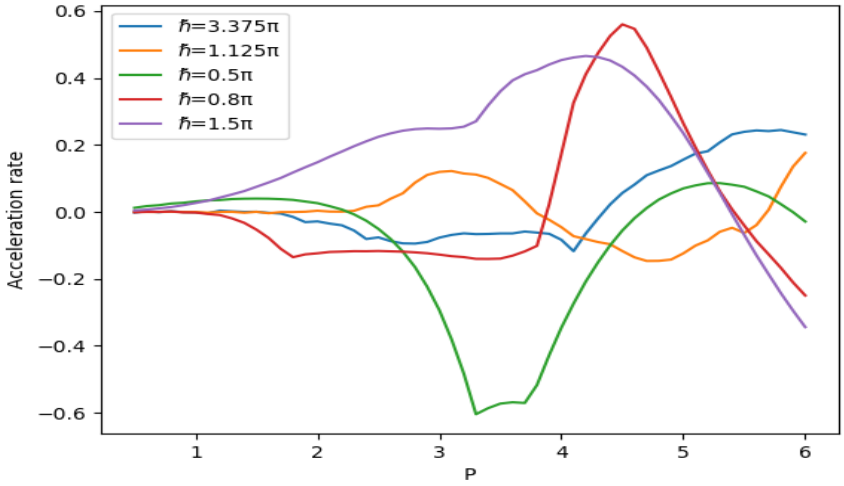

Figure 12: Acceleration rate against the potential strength

Figure 12 shows the Acceleration rate Γ of the current as a complicated function of the potential strength P for different values of the effective planck's constant $\tilde{\hbar}$ within l = 100 kicks, as a function of P, for $\tilde{\hbar}$ corresponding to a few HOQRs as well as LOQRs. From fig.12, the magnitude and direction of Γ are both seen to be tunable with P, with their P-dependence varying markedly with $\tilde{\hbar}$.

EXPLORING MORE RESONANCES

Here, we are interested in combinations of P and $\tilde{\hbar}$ that lead to optimal current. As we can see from the figures below, new resonances emerge and become higher as we increase P.

Table 2 values of highest and lowest peaks

Figure	Highest peak		Lowest peak	
16	54	$\tilde{\hbar} = 1.6\pi$	-54.6	$\tilde{\hbar} = 0.5\pi$
17	83	$\tilde{\hbar} = 1.6\pi$	-112	$\tilde{\hbar} = 0.5\pi$
18	89	$\tilde{\hbar} = 1.5\pi$	-104	$\tilde{\hbar} = 0.5\pi$
19	106	$\tilde{\hbar} = 0.8\pi$	-94	$\tilde{\hbar} = 1.25\pi$
20	129.5	$\tilde{\hbar} = 0.0\pi$	-92	$\tilde{\hbar} = 1.25\pi$

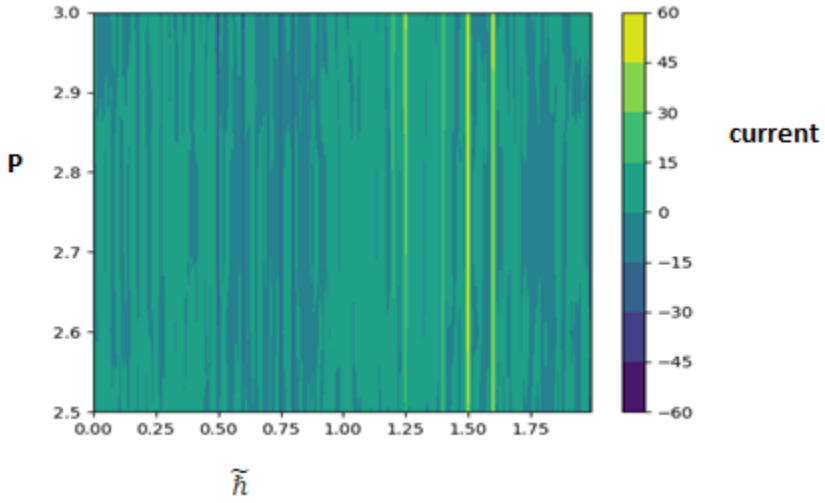

Figure 13 : Current landscape for P between 2.5 to 3.0

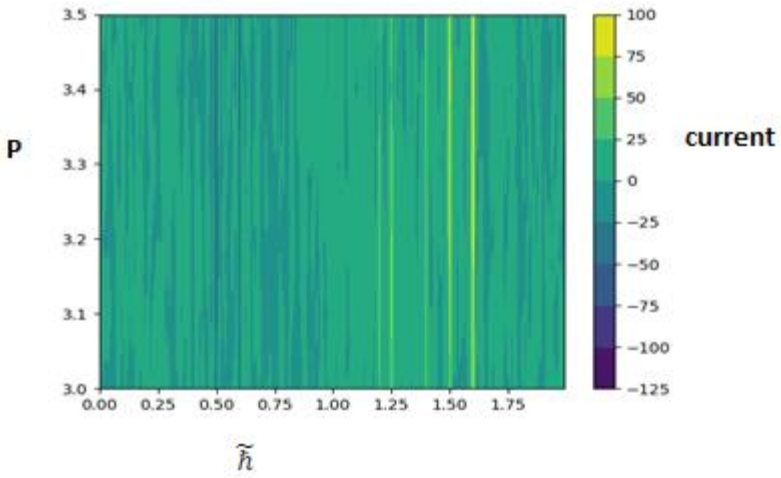

Figure 14 : Current landscape for P between 3.0 to 3.5

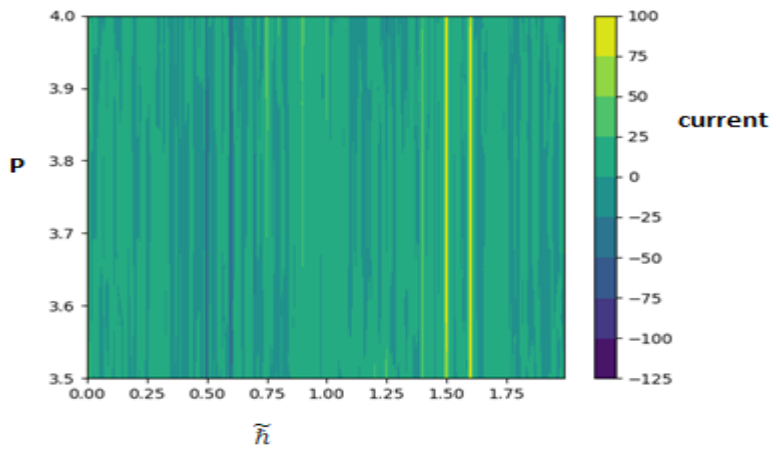

Figure 15: Current landscape for P between 3.5 to 4.0

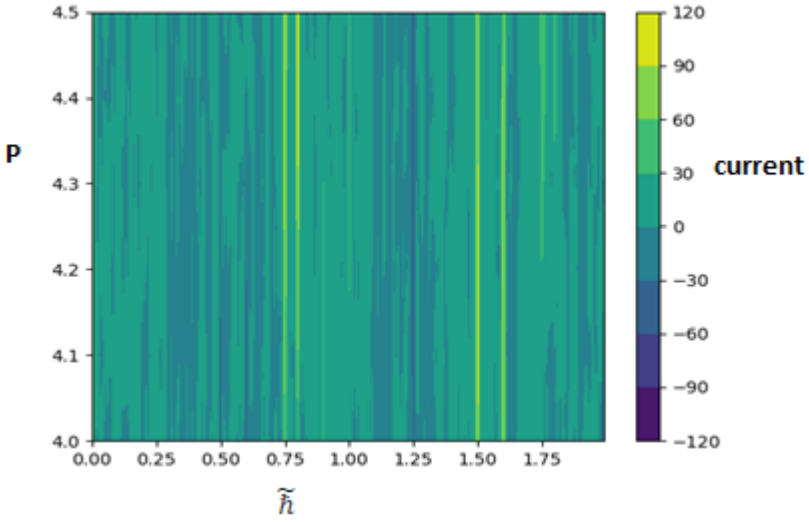

Figure 16: Current landscape for P between 4.0 to 4.5

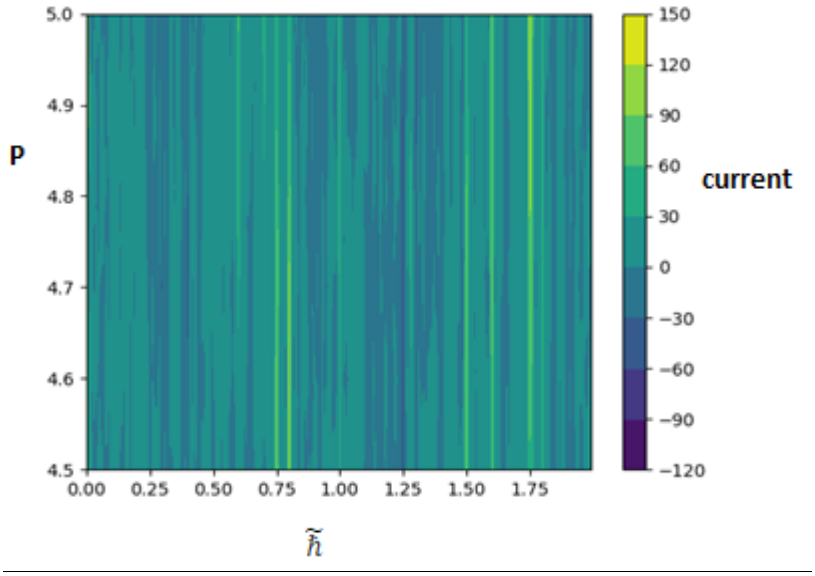

Figure 17 : Current landscape for P between 4.5 to 5.0

NUMBER OF CURRENT PEAKS

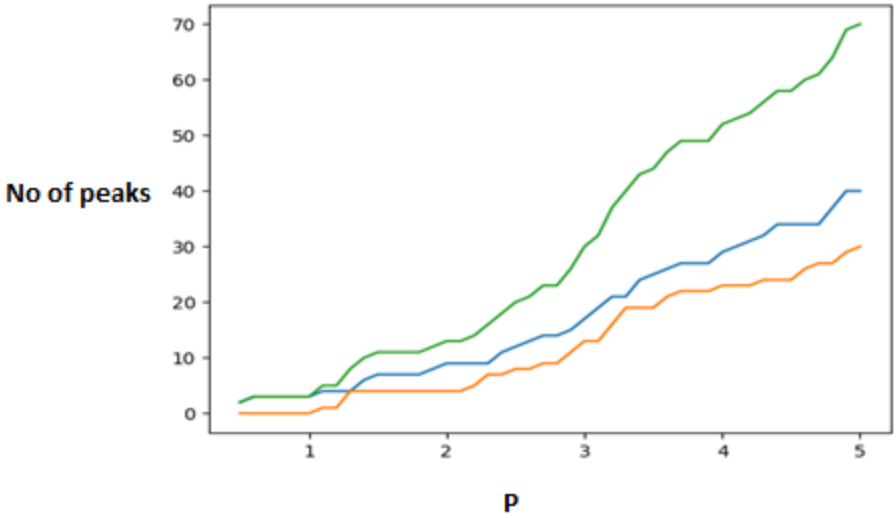

Figure 18 : Number of Peaks against P

In figure 21, the green line represents the total number of peaks as the potential is tuned. The blue line represents the number of positive against P while the orange line represents the number of negatives against P. we can make the following obvious observations

1. There are always more equal or more positive peaks than negative peaks.
2. The orange line starts off from zero when P was low and hence no current reversal.
3. All the three curves have more or less the same shape

As we would expect, the number of peaks in all the three curves monotonically increase for increasing P as more chaos appear.

THE PHASE ANGLE

In this part of the thesis, we incorporated a phase angle on the potential. The new potential is now of the form:

$$V = \sin x + \alpha \sin(2x + \theta)$$

Where θ is the phase angle of the potential

From figures 19, 20 and 21 below, it is clear that the current is affected very much by the phase angle θ. For lower values of P as we can see from figure 19, the effect of θ on the optimal current could be ignored. But as P is strengthened, θ becomes more significant. This is evident in figures 20 and 21 where the maximum values of the current deviate significantly from $\theta = 0$.

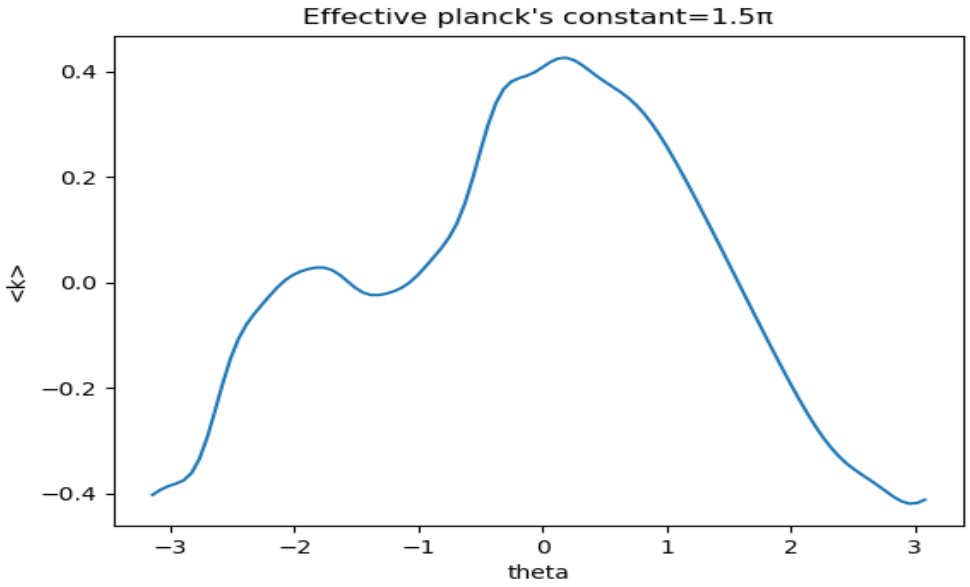

Figure 19: Optimal Current as a function of θ for P=0.5

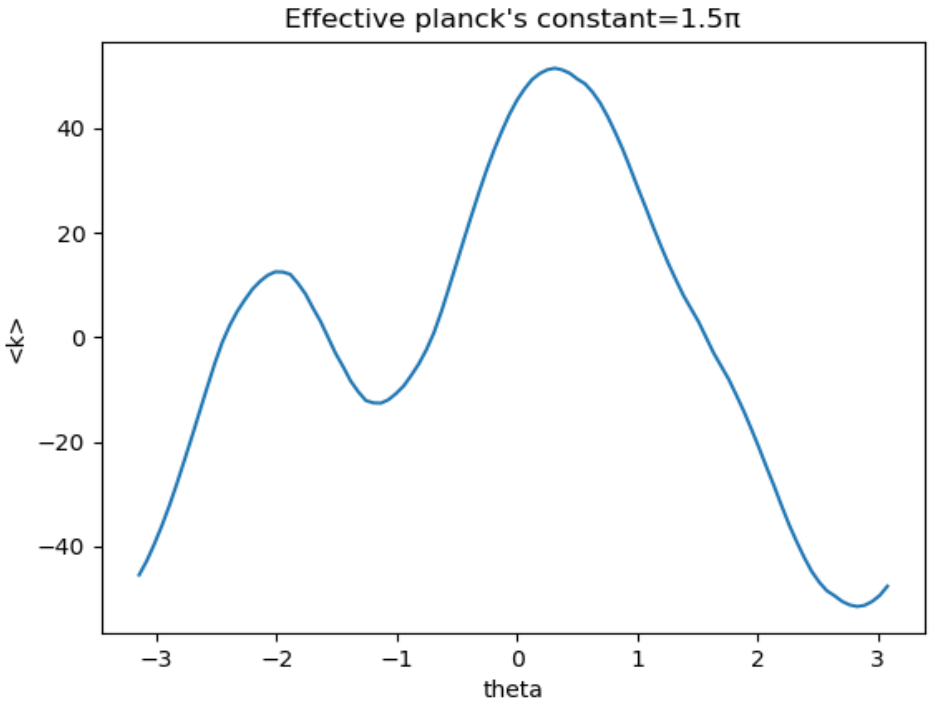

Figure 20 : Optimal Current as a function of θ for P=4.0

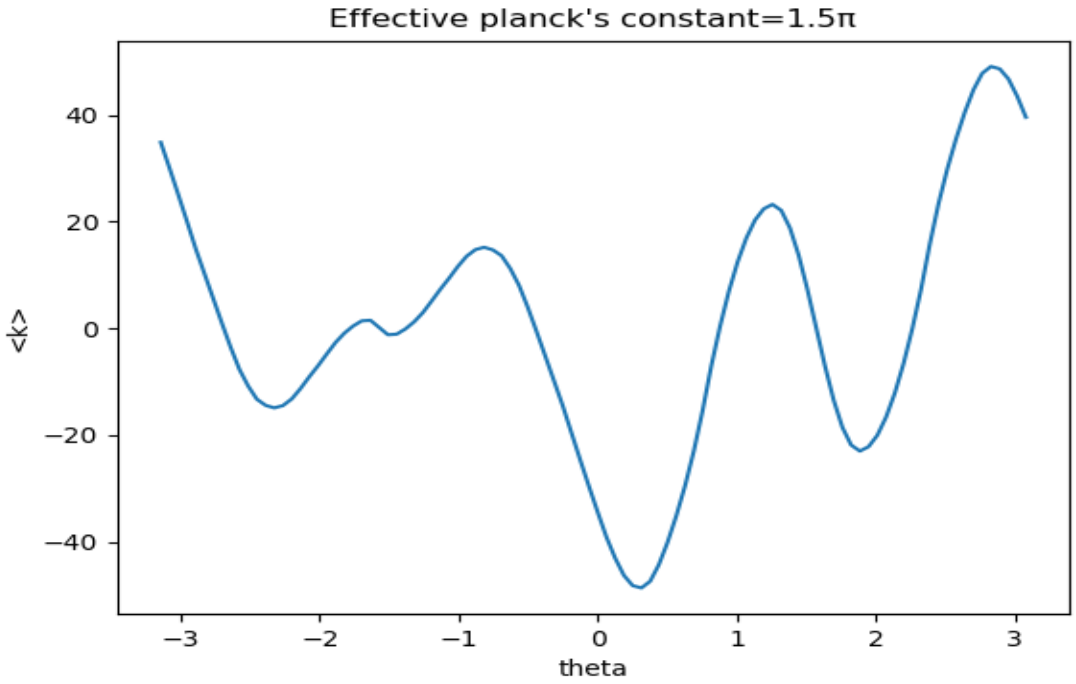

Figure 21: Optimal Current as a function of θ for P=6.0

We are therefore interested in finding out how P and θ affect these maximums. In the case where $\tilde{\hbar} = 0.5\pi$, these maximums elevate as we increase P, until a particular value is reached.(see figure).

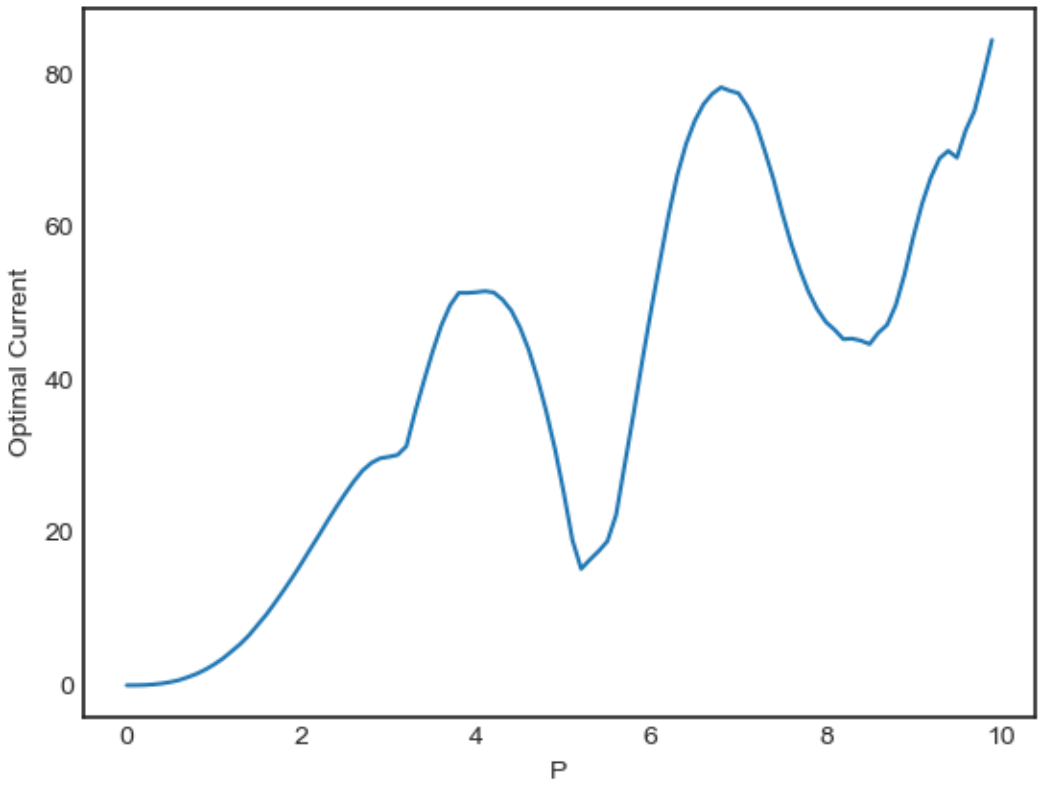

Figure 22: Optimal Current as a function of P

A similar signature can be observed on the phase angle. From figure below, it is seen that both the phase and P have critical values (θ=0.31, P=4.1) which shoots up the maximum current. A Higher critical value (θ=2.95, P=6.8) lead to higher optimal currents. This behavior seems to repeat itself as P is increased.

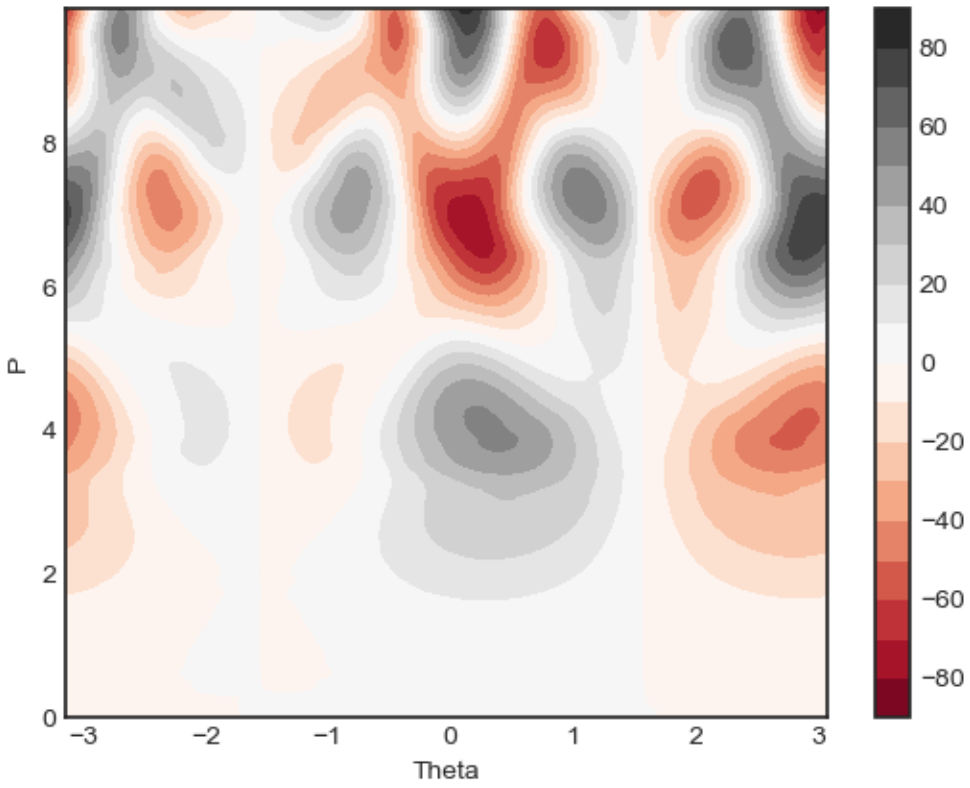

Figure 23: Optimal Current as a function of P and Θ

CHAPTER 5

SUMMARY AND CONCLUSION

This thesis has provided a firm foundation by explaining the basis of Laser cooling, Symmetry analysis of a Ratchet effect, The Ratchet effect itself, BECs and quantum resonance.

It has also shown the important role of quantum resonances of very high orders in a QKR-based quantum ratchet. The associated transport can be manipulated by use of these high-order quantum resonances.

This thesis has also partially explained that the transport associated with HOQRs become important only if the associated classical phase space is fully chaotic. The results are of great experimental interest because

(i) They offer a ratchet acceleration mechanism previously not noticed and

(ii) Suggest a new means of detecting the intriguing quantum high-order resonances in QKR systems.

It has also explored new resonances and the rapid increase in the number of resonant peaks as a result of chaos.

Finally, it has explored the influence of phase angle on the ratchet current. This study should help design new means of controlling the dynamics of cold atoms in pulsed optical lattices.

BIBLIOGRAPHY

1. Smoluchowski, M. Experimentell Nachweisbare, der Ublichen Ther- ¨ modynamik Widersprechende Molekularph¨anomene. Physikalische Zeitschrift 13 (1912), 1069–1080. reprinted in Pisma Mariana Smoluchowskiego 2, 1 (1927), 226-251
2. Feynman, R. The Feynman Lectures, vol. 1. Addison-Wesley, 1964.
3. Edris, Soliman; (2019) The Ratchet Effect with cold atoms
4. Gorre, L., Ioannidis, E., and Silberzan, P. Rectified Motion of a Mercury Drop in an Asymmetric Structure. EPL (Europhysics Letters) 33, 4 (1996), 267.
5. Switkes, M., Marcus, C. M., Campman, K., and Gossard, A. C. An Adiabatic Quantum Electron Pump. Science 283, 5409 (1999), 1905– 1908.
6. Rahman, A., Sanyal, M. K., Gangopadhayy, R., De, A., and Das, I. Evidence of a Ratchet Effect in Nanowires of a Conducting Polymer. Phys. Rev. B 73 (Mar 2006), 125313.
7. Ganichev, S. D., Tarasenko, S. A., Olbrich, P., Karch, J., Hirmer, M., Mller, F., Gmitra, M., Fabian, J., Yakimova, R., Lara-Avila, S., Kubatkin, S., Wang, M., Vajtai, R., Ajayan, P. M., Kono, J., and Drexler, C. Magnetic Quantum Ratchet Effect in Graphene. Nature Nanotechnology 8 (June 2013), 104–107
8. Letokhov, V. S. Narrowing of the Doppler Width in a Standing Light Wave. JETP Lett. 7 (1968), 272.
9. Anderson, M. H., Ensher, J. R., Matthews, M. R., Wieman, C. E., and Cornell, E. A. Observation of Bose-Einstein Condensation in a Dilute Atomic Vapor. Science 269, 5221 (1995), 198–201.
10. Kasevich, M., and Chu, S. Atomic Interferometry using Stimulated Raman Transitions. Phys. Rev. Lett. 67 (Jul 1991), 181–184.
11. Denisov, S., Morales-Molina, L., Flach, S., and Hanggi, P. ¨ Periodically Driven Quantum Ratchets: Symmetries and Resonances. Phys. Rev. A 75 (Jun 2007), 063424.

12. Denisov, S., Morales-Molina, L., and Flach, S. Quantum Resonances and Rectification in AC-Driven Ratchets. EPL (Europhysics Letters) 79, 1 (2007), 10007.
13. Salger, T., Kling, S., Hecking, T., Geckeler, C., MoralesMolina, L., and Weitz, M. Directed Transport of Atoms in a Hamiltonian Quantum Ratchet. Science 326, 5957 (2009), 1241–1243.
14. Abo-Shaeer, J. R., Raman, C., Vogels, J. M., and Ketterle, W. Observation of Vortex Lattices in Bose-Einstein Condensates. Science 292, 5516 (2001), 476–479.
15. Raman, C., Abo-Shaeer, J. R., Vogels, J. M., Xu, K., and Ketterle, W. Vortex Nucleation in a Stirred Bose-Einstein Condensate. Phys. Rev. Lett. 87 (Nov 2001), 210402.
16. Villegas, J. E., Savel'ev, S., Nori, F., Gonzalez, E. M., Anguita, J. V., Garc´ıa, R., and Vicent, J. L. A Superconducting Reversible Rectifier That Controls the Motion of Magnetic Flux Quanta. Science 302, 5648 (2003), 1188–1191
17. Shalom, D. E., and Pastoriza, H. ´ Vortex Motion Rectification in Josephson Junction Arrays with a Ratchet Potential. Phys. Rev. Lett. 94 (May 2005), 177001.
18. Grynberg, G., Lounis, B., Verkerk, P., Courtois, J.-Y., and Salomon, C. Quantized Motion of Cold Cesium Atoms in Two- and Three-dimensional Optical Potentials. Phys. Rev. Lett. 70 (Apr 1993), 2249–2252.
19. E. Lundh and M. Wallin, Phys. Rev. Lett. 94, 110603 (2005).
20. G. Ritt et al., Phys. Rev. A 74, 063622 (2006)
21. Manfred Lein, Atoms and Molecules in Strong Laser Fields: Double Ionization, Dissociative Ionization, and Harmonic Generation (2001).
22. Anatole Kenfack , Jiangbin Gong, and Arjendu K. Pattanayak, Phys. Rev. Lett. 100, 044104 (2008)
23. C. Ryu et al., Phys. Rev. Lett. 96, 160403 (2006)
24. F. M. Izrailev and D. L. Shepelyanskii, Theor. Math. Phys.43, 553 (1980).
25. J. F. Kanem et al., Phys. Rev. Lett. 98, 083004 (2007).

26. The transition to chaos: Quantum manifestations, L.E. Reichl, Springer-Verlag, NY, 2004.
27. M. Grifoni et al., Phys. Rev. Lett. 89, 146801 (2002); J. B. Majer et al., Phys. Rev. Lett. 90, 056802 (2003).